INSTITUTE OF PHYSICS PUBLISHING JOURNAL OF MICROMECHANICS AND MICROENGINEERING

J. Micromech. Microeng. **16** (2006) 920–928 doi:10.1088/0960-1317/16/5/007

# A conductivity-based interface tracking method for microfluidic application

**Juan David Salgado, Keisuke Horiuchi and Prashanta Dutta**

School of Mechanical and Materials Engineering, Washington State University, Pullman, WA 99164-2920, USA

E-mail: dutta@mail.wsu.edu

Received 12 September 2005, in final form 6 February 2006
Published 28 March 2006
Online at stacks.iop.org/JMM/16/920

**Abstract**

A novel conductivity-based interface tracking method is developed for 'lab-on-a-chip' applications to measure the velocity of the liquid–gas boundary during the filling process. This interface tracking system consists of two basic components: a fluidic circuit and an electronic circuit. The fluidic circuit is composed of a microchannel network where a number of very thin electrodes are placed in the flow path to detect the location of the liquid–gas interface in order to quantify the speed of a traveling liquid front. The electronic circuit is placed on a microelectronic chip that works as a logical switch. This interface tracking method is used to evaluate the performance of planar electrokinetic micropumps formed on a hybrid poly-di-methyl-siloxane (PDMS)-glass platform. In this study, the thickness of the planar micropump is set to be 10 $\mu$m, while the externally applied electric field is ranged from 100 V mm$^{-1}$ to 200 V mm$^{-1}$. For a particular geometric and electrokinetic condition, repeatable flow results are obtained from the speed of the liquid–gas interface. Flow results obtained from this interface tracking method are compared to those of other existing flow measuring techniques. The maximum error of this interface tracking sensor is less than 5%, even in an ultra low flow velocity.

(Some figures in this article are in colour only in the electronic version)

## 1. Introduction

Microfluidic devices are getting increasingly popular due to advances in micro/nanofabrication techniques [1–3]. Applications for such microfluidic devices range from the sensing and analysis of chemical substances to the transport of fluid in an ultra low volume. By reducing the size of fluidic devices, power consumption, reagent quantity and analysis time can be minimized. Another very important advantage of using microfluidic devices is the relatively inexpensive fabrication techniques used to construct these devices using various lithographic techniques.

Promises of microfluidic devices are almost endless [3]. Since the inception of this concept, a number of research groups have been working on the development of microdevices for micro total analytical systems ($\mu$TAS) on glass, quartz, fused silica and polymeric surfaces [1–4]. The general trend in microfluidics is not only to scale down the channel size, but also to integrate multiple functionalities for effective operations of the chip. One of the main functionalities is on-chip detection of flow and macromolecules. In the literature, there exist a number of on-chip flow measuring techniques based on thermal anemometry [5–9], pulse modulation [10], electromagnetic principles [11], etc. These methods can be used to measure the flow velocity in steady, fully developed and completely wetted microchannels. However, their usage cannot be extended to estimate the marching velocity of traveling liquid front in a microchannel.

The study of marching velocity in microfluidic channels or capillaries is important to determine the surface energy [12], electrowetting (electrocapillary) [13] and other charge-related wetting phenomena [14]. Yang *et al* have determined the surface tension force and contact angle by detecting the instantaneous position of traveling liquid front [15]. Through an identical procedure, Tas *et al* measured the filling speed of water in nanofluidic channel, and found that the electro-viscous effect plays an important role in wetting nanochannel

  

[16]. In these works, an optically based method is used to track the instantaneous location of liquid in micro/nanochannel or capillary surface. However, optical techniques cannot be used if the microchannel material is opaque. Even in transparent microchannels, an optical method normally requires relatively large and expensive equipments (high speed camera, objective lens, appropriate light source, color filter, precisely controlled traversing mechanism, etc) which are major bottlenecks for the on-chip concept. In this paper, we present a novel interface tracking method that works on the basis of the measurement of conductivity of wetting liquids. This on-chip interface tracking velocimetry is minimally intrusive, very sensitive, less expensive and a more reliable method for detecting liquid–gas interface in a microchip of characteristic dimension as small as 1 $\mu$m. Here, the conductivity-based interface tracking method is used to quantify the driving/filling capability of electroosmotic flow in an unwetted PDMS-glass microchannel. To our knowledge, no other study (until today) used an electroosmotic technique to investigate the wetting phenomena in microchannel networks. This conductivity-based interface tracking method can easily be applied to find the velocity of gas–liquid interface in phase change micropump [17, 18], thermocapillary micropump [19], micro heat exchanger [20] and microchip blood viscometer [21].

This paper is organized as follows: in the next section, the design of our conductivity-based interface tracking device is introduced along with planar electroosmotic pumping. In the following section, electrokinetic theory and numerical simulation results are presented to identify the optimum separation distance between field electrodes. This is followed by the microfabrication methods for making an on-chip interface tracking device. Finally, flow results and accuracy of conductivity-based interface tracking device are presented.

## 2. Microfluidic chip design for interface tracking velocimetry

This on-chip interface tracking device consists of a fluidic circuit and an electronic component. Figure 1 shows a schematic diagram of the fluidic circuit used in this interface tracking device. The fluidic circuit contains a microchannel, two reservoirs and a number of electrodes. The first two electrodes are named field electrodes, while the remaining electrodes are called sensing electrodes. Field electrodes are placed for on-chip electrokinetic pumping. The spacing and size of the field electrodes are predicted by numerical simulation, which is presented in the following section. The sensing electrodes are deposited along the channel to detect the existence of a liquid–gas boundary. In this study, the channel height, width and length are kept constant at 10 $\mu$m, 1 mm and 5.5 cm, respectively, and the diameter of each reservoir is 5 mm.

This interface tracking sensor basically works on the measurement of electrical conductivity between a pair of sensing electrodes. Each pair of sensing electrodes is connected to an electronic circuit. The electronic circuit, as shown in figure 2, has two major components: voltage dividers and comparator. The left voltage divider consists of a base resistance ($R_B$) and a variable resistance ($R_V$), while the right one uses two known resistances ($R_1$ and $R_2$). When

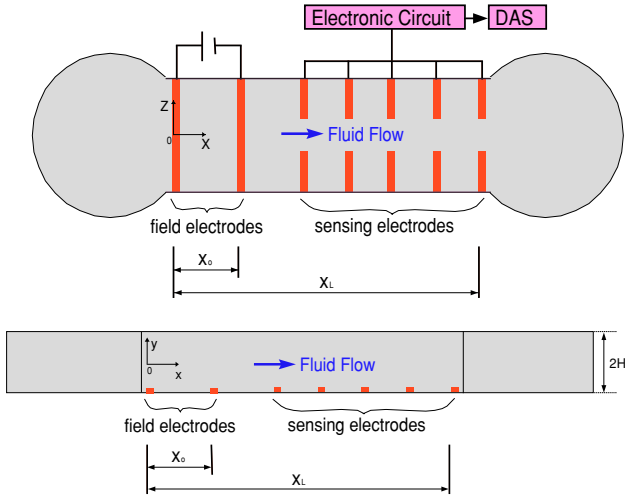


**Figure 1.** Schematic top and front views of the interface tracking sensor. The fluidic network consists of two reservoirs and a microchannel. Five pairs of sensing elements are shown to measure the velocity at five different locations along the channel, while two field electrodes are used for applying external electric fields. Here $x_0$ is the distance between two field electrodes.

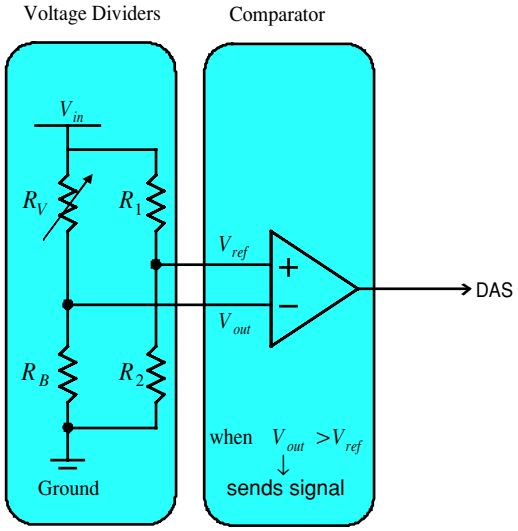


**Figure 2.** The electronic circuit used for each sensor element. Each electronic circuit is composed of two voltage dividers and a comparator. In this study $R_1 = 3$ kΩ and $R_2 = 2$ kΩ.

measuring the traveling speed of a particular liquid through the microfluidic sensor, $R_B$ is the resistance of buffer (liquid) between a pair of sensing electrodes. One can estimate the value of $R_B$ from the resistivity of the buffer and flow geometry between a pair of electrodes. For flow of di-ionized (DI) water in our interface tracking sensor, the value of $R_B$ is calculated as 2.43 MΩ.

In our experiment, voltage dividers are powered by a power source (QDR40-0.75, Raytheon Company). Conversely, for input voltage ($V_{in}$), a 5 V battery could have been attached to the electronic circuit. The reference voltage ($V_{ref}$) and output voltage ($V_{out}$) can be expressed as

$$V_{ref} = \left(\frac{R_2}{R_1 + R_2}\right) V_{in} \qquad (1)$$

$$V_{\text{out}} = \left(\frac{R_{\text{B}}}{R_{\text{V}} + R_{\text{B}}}\right) V_{\text{in}}. \tag{2}$$

In typical operations, the value of $R_1$ is set higher than the value of $R_2$. Therefore, the reference voltage will always be less than 0.5 $V_{\text{in}}$ ($0 \leqslant V_{\text{ref}} \leqslant 0.5\,V_{\text{in}}$). However, the value of the output voltage depends on the resistance of the fluid between a pair of sensing electrodes. During the flow experiment, when the buffer (liquid) touches a pair of sensing electrodes, the variable resistance, $R_{\text{V}}$, between that pair approaches the identical value of the base resistance, $R_{\text{B}}$. Hence, in contact with target liquid the output voltage ($V_{\text{out}}$) changes from 0 to 0.5 $V_{\text{in}}$. These reference and output voltages are then passed to a voltage comparator. The comparator ($\mu$A311, Fairchild) transmits a digital signal to the data acquisition system if the output voltage is higher than the reference voltage ($V_{\text{out}} > V_{\text{ref}}$). Thus, if there is no liquid between a pair of electrodes, no signal will be generated by the comparator for that pair of electrodes. The data acquisition system contains two microchips: parallel port chip (AMD P8255A) and system timing controller (AMD 9513). The function of parallel port chip is to identify the origin of the digital signal, while the system-timing controller registers the time of digital signal. From the position and time difference between two consecutive sensing elements, the flow velocity of traveling front, $V_{\text{f}}$, can be computed as

$$V_{\text{f}}|_j = \left.\frac{\mathrm{d}x}{\mathrm{d}t}\right|_j \cong \frac{x_{j+1} - x_j}{t_{j+1} - t_j} \tag{3}$$

where $x$ is the location of sensing element, $t$ is the time recorded by the electronic circuit, and $j$ is the index for a particular sensing element. As the fluid front passes through the microchannel, it will come in contact with each electrode pair. Thus, the interface tracking device will generate a series of signals, and the time of each signal is recorded in a computer program for velocity measurement. In this study, a solderless breadboard (EIC-106, EIC) is used to construct all electronic circuits, and each electronic circuit is properly wired to a pair of sensing electrodes. Eleven pairs (only five pairs shown in figure 1) of sensing electrodes are utilized to obtain the flow velocity along the microchannel. Depending on the system requirements, the number of sensing elements can be increased or decreased.

### 2.1. Field electrodes for planar electrokinetic micropumps

The specific objective of this section is to present a design for field electrodes that can provide uniform electric fields for electrokinetic flow, but offer very minimal flow resistances. In electrokinetic pumping, field electrodes are generally placed vertically in the inlet and exit reservoirs. The vertical arrangement of electrodes guarantees a uniform electric field in the channel, especially in the straight channel. However, for electrodes within a channel, it provides the maximum flow impedance as it directly blocks the flow path. In order to minimize flow disturbance, all electrodes are placed on the bottom glass substrate and the thickness of the electrodes is maintained below 100 nm. It is important to note that the surface roughness of PDMS and commercial cover glass surfaces (Microscope Slides, Fisher Scientific) varies between 50 nm and 100 nm. Therefore, the placement of 100 nm thick electrodes in the flow path does not contribute to flow impedance significantly if the channel height is 1 $\mu$m or higher.

*2.1.1. Governing equations for electrokinetic motion.* The incompressible electroosmotic flow is governed by Navier–Stokes equation as [22]

$$\rho_{\text{f}} \frac{\mathrm{D}\vec{V}}{\mathrm{D}t} = -\nabla P + \mu \nabla^2 \vec{V} + \vec{F}_{\text{B}} \tag{4}$$

where $\rho_{\text{f}}$ is the fluid density, $\vec{V} = (u, v)$ is the velocity field, $P$ is the pressure, and $\mu$ is the dynamic viscosity. The body force ($\vec{F}_{\text{B}}$) originates from the interaction of electric charge density ($\rho_{\text{e}}$) and externally applied electric field is given by

$$\vec{F}_{\text{B}} = -\rho_{\text{e}} \nabla \phi. \tag{5}$$

The externally imposed electric potential ($\phi$) is governed by [22]

$$\nabla (\sigma \nabla \phi) = 0 \tag{6}$$

where $\sigma$ is the conductivity. This potential is subjected to zero flux conditions at the boundary. In microchannel applications, the electric charge density ($\rho_{\text{e}}$) decays exponentially within the electric double layer (usually 3–10 nm from the channel surface) [22]. Hence, body forces ($\vec{F}_{\text{B}}$) will be significant if and only if there is a strong electric field next to the channel surface. In a straight microchannel, the electric fields are generally uniform if the field electrodes are placed throughout the channel cross-section. However, in this study, the height of microelectrodes is only 1/100th of the channel height. Therefore, we would expect significantly small electric field values, particularly in the electric double layer region of top (PDMS) wall, if the separation distance between field electrodes is very small. In the following section, numerical simulation results are presented to identify the optimum locations of field electrodes in the microchannel for electroosmotic pumping.

*2.1.2. Simulation of electric fields.* In this section, the electric field lines are simulated for different separation distances between field electrodes. An h/p-type spectral element method is used to calculate electric fields in streamwise and cross-stream directions [23]. This numerical algorithm employs modal spectral expansion in quadrilateral and unstructured triangular meshes. Details of the numerical scheme and convergence results are presented in [23].

Figure 3 shows the electric field lines ($\vec{E}$) and the streamwise electric field ($E_x$) distribution between anode and cathode for different field electrode configurations. All numerical results are presented in non-dimensional form, where $\xi = x/H$, $\eta = y/H$, and $H$ is the half channel height. For instance, in a 10 $\mu$m deep channel, $H$ is 5 $\mu$m. Here the height of each field electrode is set to be 100 nm ($\eta = -1$ to $-0.98$), while the separation distance between field electrodes is varied from case to case. In figure 3($a$), the non-dimensional separation distance between two field electrodes is 100 (0.5 mm), and uniform electric fields are obtained for this case. However, the electric field distribution changes significantly if the separation distance between the two field electrodes decreases as shown in figures 3($b$) and ($c$). As the separation

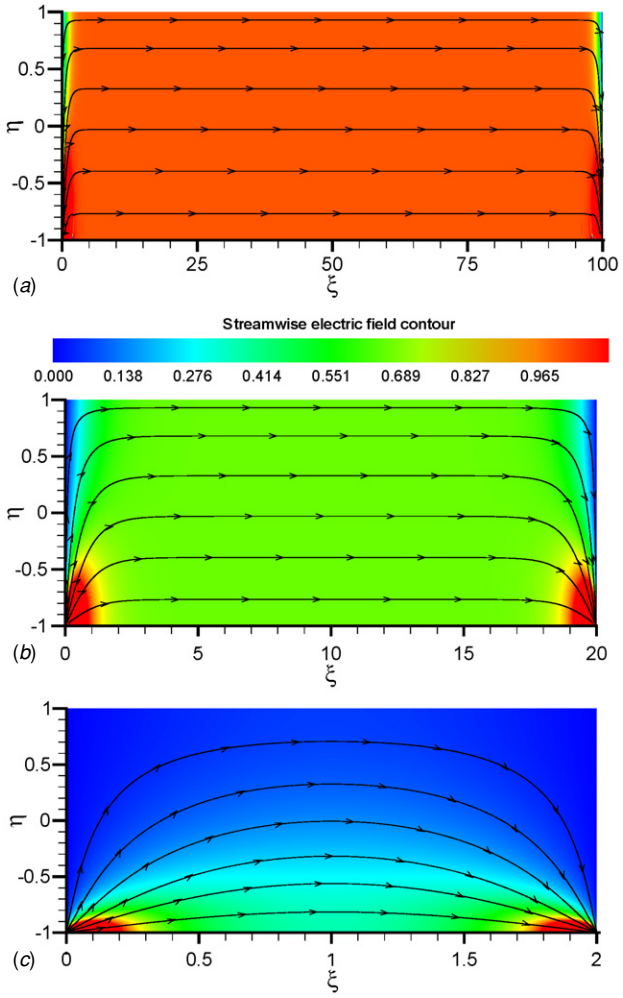


**Figure 3.** Streamwise electric field distribution in a microchannel. An h/p-type spectral element method is used to predict the electric potential and field distribution. The separation distances between field electrodes are (*a*) 0.5 mm, (*b*) 0.1 mm and (*c*) 10 $\mu$m.

distance gets smaller, the electric field line deviates further from their uniform structure, especially at the area close to the top wall ($\eta = 1$). Figure 4 illustrates the non-dimensional streamwise electric field distribution ($E_x^* = E_x/E_\mathrm{b}$) along the channel height ($y$) direction at $x = 0.5x_0$. Here $E_\mathrm{b}$ is the ideal streamwise electric field, and it can be expressed as

$$E_\mathrm{b} = [\phi(x_0) - \phi(0)]/x_0.$$

Numerical results show that for electrode separation distance of $20H$ or higher, the electric field lines become uniform across the channel. The magnitude of the electric field is much smaller if the electrodes are very close. For example, if the separation distance between two electrodes is $20H$, the electric field strength is only 66% of the expected (ideal) value. However, the non-dimensional electric field value approaches unity once the separation distance between two field electrodes becomes $2000H$. Therefore, on the basis of the numerical results, the separation distance between two field electrodes is set to be 10 mm in order to obtain uniform electric field in the microchannel, especially very close to the top (PDMS) wall.

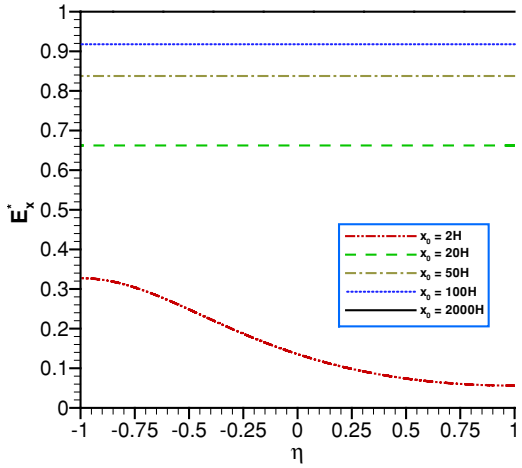


**Figure 4.** The non-dimensional electric field distribution along the $y$-direction at the mid-plane between two field electrodes for different electrode separation distances.

## 3. Fabrication of the microfluidic chip

Fabrication techniques for the micro-electro-mechanical systems (MEMS) and microfluidics are derived from standard processes used in the formation of the semiconductor devices. These microfabrication processes include lithography, etching and thin-film deposition [24]. These well-established techniques have guided researchers to select optical grade glass and quartz as device materials. In the past few years, polymeric-based materials, such as poly-di-methyl-siloxane (PDMS), polymethyl-methacrylate and poly-carbonate have received more attention as device materials, since devices made of these (polymeric) materials can be mass-fabricated using injection molding, embossing or imprinting, laser ablation and soft lithography [25]. In this study, PDMS is used to form the channel structure due to its ease of fabrication, integration and low cost, while electrodes are deposited on a glass substrate. Note that it is possible to form electrodes on a PDMS layer using sputtering techniques, but the glass substrate provides a rigid structure for the whole microfluidic chip.

### *3.1. Microfabrication schemes*

Soft lithography technique is used to form the channel and reservoir structure on PDMS. This technique offers rapid prototyping, easy multilayer fabrication, shorter turn-out time, mass scale production and cheaper device cost [26, 27]. Figure 5 shows the microfabrication schemes used in this study. First, a glass substrate is cleaned with acetone, DI water and iso-propyl alcohol (IPA) and dried with compressed air for photolithography process. Photoresist (AZ 4620, Clariant), on the order of the channel thickness, is then spin-coated on the planar glass substrate. The thickness of the photoresist can be varied from 1 to 10 $\mu$m by changing the spin rate and duration. This is followed by softbaking the photoresist on a hotplate (Model 04744, Cole Parmer) for 5 min at 70 °C. The photoresist is then illuminated under UV light for 60 s to make a positively etched channel pattern. Using a photoresist developer (AZ 400, Clariant), the illuminated photoresist

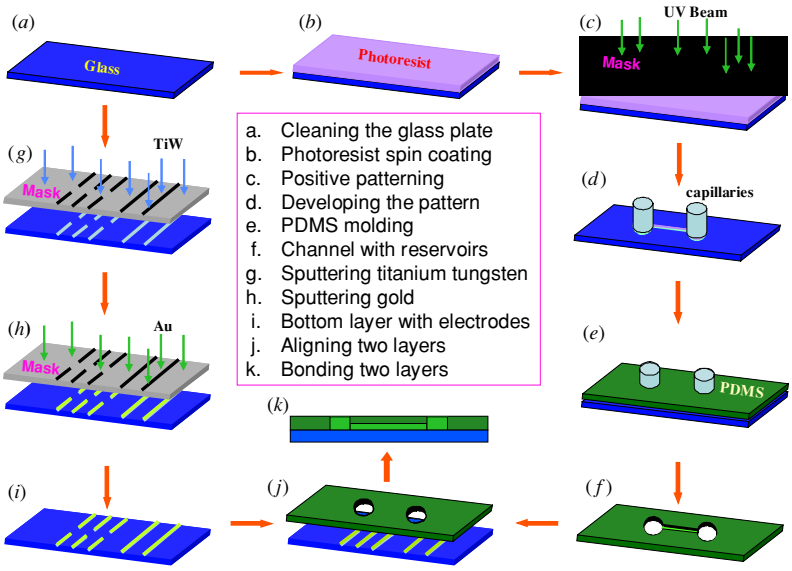


**Figure 5.** Microfabrication sequences used for fabricating on-chip interface tracking sensors.

is carefully dissolved. At the end of the photolithography process, the photoresist is rinsed with DI water and blow dried with compressed air. Once the glass microslide has the positive pattern of the sample channel, two capillaries are attached at the reservoir locations. Next, base and curing agent of PDMS (Sylgard 184, Dow Corning) are mixed at a ratio of 10:1, and then degassed in a vacuum desiccator for 1 h. The liquid polymer is then poured onto the positively patterned mold and left to cure at 80 °C for 6 h. At the end of the curing process, the PDMS layer is peeled off from the glass substrate, and the sample is submerged in acetone for 2 h. Then the PDMS layer is rinsed with DI water and IPA, and blow dried with the compressed air. This PDMS layer is used as the top surface of the integrated microfluidic network.

For fabricating electrodes and sensing elements, 5 nm of titanium tungsten (TiW) is sputtered on a cover glass followed by 95 nm of gold (Au). Here, titanium tungsten is deposited as a binding agent since the bonding strength between glass and gold is very weak. Sputtering is carried out in the dc mode for 23 min under a chamber pressure of $7.5 \times 10^{-3}$ Torr and argon is introduced at a flow rate of 8.16 ml $\text{min}^{-1}$. In the sputtering process, the power levels for TiW and Au are set at 100 W and 75 W, respectively. In order to minimize the flow disturbances due to electrodes, the total film thickness is restricted to 100 nm.

In the microchip, the exact positioning of electrodes is very important in quantifying electric fields and flow velocities along the microchannel. Therefore, electrodes are created by precise patterning of photoresist (AZ4620) and selective etching of gold and TiW thin films from the glass substrate. The photolithography technique used during patterning process is identical to that described earlier, but in this case a different mask is used (not shown here) to form an array of electrodes. In the etching processes, trifluoric acetic acid (TFA) and 30% hydrogen peroxide are used to remove gold and titanium tungsten, respectively. The sample is then rinsed with DI water, acetone and IPA and blow dried with compressed air.

Next, both the top (PDMS) and the bottom (glass) layers are placed in oxygen plasma (PDC-32G, Harrick Scientific Corporation) for a couple of minutes. The function of the plasma cleaner is not only to remove any dust/organic particles, but also to activate the surfaces of PDMS and glass for chemical bonding. Both layers are then cured further by aligning them properly until they bond together. This hybrid microchip is then rinsed with Nanopure water for several times. Finally, the water is removed from the microchip using compressed nitrogen gas, and the chip is stored at room temperature for at least 7 days so that the spontaneous hydrophilic action disappears from the PDMS surfaces [28].

## 4. Experimental section

### *4.1. Experimental uncertainty*

A detailed uncertainty analysis is performed for this experimental study. The overall uncertainty of an experimentally measured variable is calculated as (for details see [29])

$$U_i = \sqrt{B_i^2 + P_i^2} \tag{7}$$

where $B_i$ is the systematic or bias error and $P_i$ is the precision or random error of the measured variable $i$. The variables measured in this experiment are sensor location, sensing time, input voltage of the power source and the electric current. In our experiments the bias error was very small compared to the precision error. The error propagation equation developed by Kline and McClintok [30] is used to calculate the uncertainties of flow velocity, discharge and pressure. The uncertainties of this experimental work are summarized in table 1.

### *4.2. Flow experiment*

In this study, electroosmotically induced pressure is used to drive a liquid along the microchannel. In order to obtain an electroosmotic driving mechanism, the microchannel is

**Table 1.** Uncertainty values of different experimental parameters.

| Input parameter | Absolute uncertainty | Output parameter | Relative uncertainty (%) |
|---|---|---|---|
| Position ($\mu$m) | $\pm$10.0 | Velocity | $\pm$5.69 |
| Time (ms) | $\pm$1.0 | Discharge | $\pm$5.84 |
| Voltage (kV) | $\pm$0.01 | Pressure | $\pm$5.94 |
| Current (nA) | $\pm$1.0 | | |

first filled with de-ionized water from the left reservoir to the second field electrodes using compressed nitrogen. An electric field is then applied between two field electrodes from a dc power supply (HV-30-P, Unimicro Technologies, Inc.). The flow experiments are performed at least 7 days after the plasma cleaning of PDMS surfaces, and no spontaneous filling action is observed in our microfluidic system. This means that the surface tension force was not large enough to overcome the frictional resistances offered by the wetted section of the microchannel. This finding is consistent with recent experimental study of Yang *et al* [15]. In their study, it was shown that in a polymeric microchannel, the pressure differential across the liquid–gas interface is much smaller than the external pressure gradient for the first time filling of water. Hence, we neglect the surface tension effects in the analysis of experimental data. However, surface tension effects may be dominant if the surface is oxidized [28] or electrical properties of the surface are modified [14].

As mentioned in the fabrication section, our microchannel is made of PDMS and glass. Both PDMS and glass generally acquire negative charges on their surface when they come in contact with DI water. Hence, the electric double layer will have a net positive charge, and an externally applied positive electric field will result in a net flow of positive ions from anode to cathode that will drag the surrounding liquid particles from left to the right direction [23]. It is noteworthy to mention that the applied electric field and the resultant body force will only be active between the two field electrodes ($0 \leqslant x \leqslant x_0$).

The flow between the two field electrodes will not be purely electroosmotic once the fluid passes the second field electrode, rather it will be mixed electroosmotic and pressure driven. In this mixed flow case, the mean flow velocity is less than the pure electroosmotic velocity for identical electric field strength [23]. This is due to the fact that an adverse pressure gradient is created between two field electrodes. For a low Reynolds number ($Re \ll 1$) microflow in a two-dimensional (planar) channel, the induced pressure at the end of the second electrode ($x = x_0$) can be expressed as [31]

$$P_0^{\mathrm{M}} = \frac{3x_0\mu}{H^2}\left(\frac{\varepsilon\zeta E_x}{\mu} - u_{\mathrm{m}}\right) = \frac{3x_0\mu}{H^2}(ME_x - u_{\mathrm{m}}) \qquad (8)$$

where $\zeta$ is the zeta potential, $M$ is the electroosmotic mobility, $E_x$ and $u_{\mathrm{m}}$ are the streamwise electric field and mean velocity, respectively. The value of the zeta potential depends on the channel surface charge characteristics and ion distribution in the electrolyte solution. Hence, electroosmotic mobility, $M = \varepsilon\zeta/\mu$, is a strong function of surface electric condition and fluid temperature.

The induced pressure relation presented in equation (8) is based on the assumption that at any particular time, the mean velocity remains constant ($u_{\mathrm{m}} = V_{\mathrm{f}}$) throughout the wetted channel. This can be justified from the fact that in microflow the time scale for unsteadiness is on the order of microseconds [32]. Since the temporal resolution of our interface tracking sensor is 1 ms, the flow velocity measured at any sensing location can be considered steady when it was recorded. Therefore, from mass continuity, the velocity will be at the same value from the inlet reservoir to the recorded point during that particular instance. From equation (8), it is clear that for a particular geometric ($H$), electrokinetic ($M$) and electric field ($E_x$) condition, the induced pressure ($P_0$) increases linearly as the mean velocity decreases. Moreover, for particular electric field strength, the induced pressure ($P_0$) increases quadratically with a decrease in channel height.

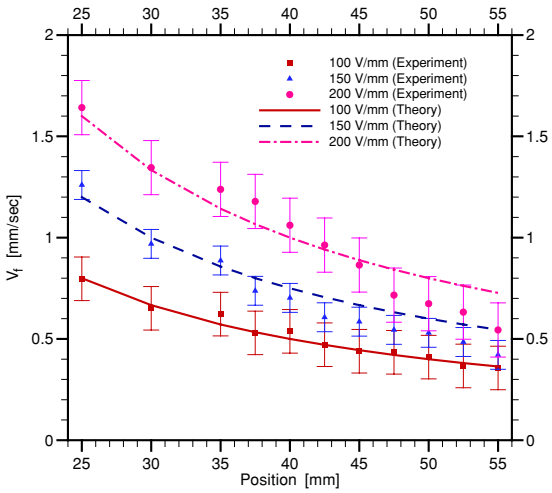


**Figure 6.** Instantaneous flow velocity registered at different sections of the microfluidic channel at various electric field strengths. Here the predicted velocity is based on a one-dimensional flow model. The electroosmotic mobility, $M = 2.0 \times 10^{-4}$ cm$^2$ (V s)$^{-1}$, is obtained from a separate experiment of pure electroosmotic microflow in a 10 $\mu$m deep PDMS-glass microchannel [33]. The flow Reynolds number of mixed flow is between $9.259 \times 10^{-3}$ and $1.434 \times 10^{-3}$.

After the second field electrode ($x_0 < x \leqslant x_{\mathrm{L}}$), there is no electroosmotic action due to the nonexistence of any electric field, though electric double layers exist throughout the fluidic network. In this region, the flow is driven by the pressure head generated from electroosmotic action. The theoretical pressure head requires driving the flow in the unwetted part of the microchannel ($x > x_0$) can be presented as

$$P_0^{\mathrm{T}} = \frac{3x_0\mu}{H^2}\left(\frac{x - x_0}{x}\right)ME_x. \qquad (9)$$

The above equation is only valid for low Reynolds number microflow. Therefore, from equations (8) and (9), one can obtain an approximate expression for marching velocity as

$$u_{\mathrm{m}} = ME_x\frac{x_0}{x}. \qquad (10)$$

Figure 6 illustrates the microflow results in a 10 $\mu$m deep channel at different electric field strengths. Here symbols represent experimental results obtained from the interface tracking device, while the solid lines show predicted velocity based on a one-dimensional flow model. In all experimental runs, the length and width of the microchannel are kept constant at 2 cm and 1 mm. The applied electric field is varied between 100 V mm$^{-1}$ and 200 V mm$^{-1}$, and no bubble

**Table 2.** Flow velocity obtained from the optical- and conductivity-based interface tracking method under identical geometric and electrochemical conditions. Verification results are presented for three different channel heights: 10 $\mu$m, 7 $\mu$m and 3.5 $\mu$m.

| | | Marching velocity | | | |
|---|---|---|---|---|---|
| | | Conductivity method | | Optical method | |
| Electric field (V mm$^{-1}$) | Channel depth ($\mu$m) | Mean (mm s$^{-1}$) | Std. Dev. (mm s$^{-1}$) | Mean (mm s$^{-1}$) | Std. Dev. (mm s$^{-1}$) |
| 100 | 10 | 0.395 227 | 0.066 943 | 0.402 413 | 0.049 953 |
| | 7 | 0.552 197 | 0.068 036 | 0.541 814 | 0.039 978 |
| | 3.5 | 1.042 648 | 0.043 470 | 1.004 133 | 0.033 396 |
| 110 | 10 | 0.511 791 | 0.064 661 | 0.502 884 | 0.026 386 |
| | 7 | 0.619 101 | 0.031 641 | 0.614 482 | 0.040 170 |
| | 3.5 | 1.134 617 | 0.039 436 | 1.119 687 | 0.062 842 |
| 120 | 10 | 0.556 596 | 0.062 786 | 0.543 117 | 0.013 456 |
| | 7 | 0.656 832 | 0.052 866 | 0.648 382 | 0.020 278 |
| | 3.5 | 1.203 697 | 0.027 848 | 1.183 497 | 0.063 447 |
| 130 | 10 | 0.610 357 | 0.020 600 | 0.617 836 | 0.027 626 |
| | 7 | 0.715 455 | 0.061 501 | 0.704 255 | 0.025 194 |
| | 3.5 | 1.332 520 | 0.057 024 | 1.338 670 | 0.112 224 |
| 140 | 10 | 0.659 946 | 0.040 419 | 0.655 460 | 0.022 530 |
| | 7 | 0.783 664 | 0.031 552 | 0.736 160 | 0.022 018 |
| | 3.5 | 1.426 447 | 0.048 521 | 1.439 297 | 0.117 353 |
| 150 | 10 | 0.746 679 | 0.037 234 | 0.730 211 | 0.031 654 |
| | 7 | 0.918 326 | 0.143 888 | 0.908 073 | 0.088 343 |
| | 3.5 | 1.492 017 | 0.031 197 | 1.574 253 | 0.207 077 |

is observed within this range. Each error bar is obtained from seven individual experimental runs with a confidence interval of $\pm 3\sigma$. The experimental results show how the flow velocity changes as the fluid moves along the downstream direction under the action of induced pressure. As the fluid travels in the downstream direction, the flow velocity registered by downstream sensors decreases. From the presented trend in the flow velocity, one can conclude that the largest flow velocity is the pure electroosmotic velocity, and the maximum possible velocity could be monitored using a sensing electrode next to the second field electrode. Experimental results also show that the microflow velocity changes in proportion to the applied electric field strength. This is because of the initial pressure building ability of the mixed flow in the electric field region. Since the driving pressure of electroosmotic flow is directly related to the electric field and zeta potential, one can expect higher flow velocity or induced pressure at the higher electric fields. The experimental results show good agreement with the one-dimensional model presented here. The difference between experimental results and theoretical prediction becomes higher as the electric field is increased. This could be attributed to the slight increase in mobility at the higher electric field region due to Joule heating [34].

### *4.3. Sensor accuracy*

In this study, both pressure and electroosmotically driven microflows are used to verify the accuracy of the conductivity-based interface tracking method. At an ultra low flow velocity ($V_f < 2$ mm s$^{-1}$), the fluid is driven by electrokinetic body forces between two field electrodes. In this case, the flow velocities obtained from our sensor are compared to those of an optical-based interface tracking method [15, 16]. For the verification run, the microchannel is mounted on the stage of an inverted microscope (CKX41, Olympus, Japan) equipped with a 1280 × 1024 × 12 bit CCD camera (PIVCAM 13-8, TSI, Inc.). Images are continuously captured by software (Insight, Version 3.20, TSI, Inc.). Using a 20× objective lens, a field of view on the monitor is calculated as 429 × 344 $\mu$m with a ratio of 0.335 $\mu$m per pixel. Electric potentials are then applied up to 1500 V between the first two field electrodes from a high voltage power supply. Times of flight are recorded for both optical- and conductivity-based interface tracking methods when the interface between air and water passes the preset reference points in the flow channel. Flow velocities obtained from the verification run are presented in table 2. For the ultra low flow velocity, our conductivity-based sensor is able to calculate within 5% of the optical-based interface tracking method.

For higher flow rates, pressure-driven flows are utilized to verify the accuracy of the interface tracking sensor. Here a syringe pump (74900 series, Cole-Parmer, Inc.) is used to drive the flow from the inlet to the exit reservoir. In this case, three pairs of sensing electrodes are placed vertically at the exit reservoir. In order to obtain accurate flow velocity, the sensing electrodes are deposited on a glass microslide using sputtering techniques, and the glass plate is placed in the exit reservoir using a 2D positioning platform. The separation distance between sensing elements is set at 100 $\mu$m. For pressure-driven flow experiments, the diameter of the exit reservoir is 1 cm, while other dimensions are the same as for the flow experiment (presented in the earlier section). Relatively high flow rates (in excess of 100 $\mu$l min$^{-1}$) are used to measure the steady discharge in the microchannel. The error in experimental results is quantified as

$$\text{Abs error} = \frac{|Q_A - Q_S|}{Q_A} \times 100\% \qquad (11)$$

where $Q_S$ and $Q_A$ are the flow rates from the microfluidic sensor and the syringe pump, respectively. Figure 7 shows the error distribution at different flow rates. Each error point is based on five individual runs under the same operating conditions. At the higher flow rates, experimental flow results obtained

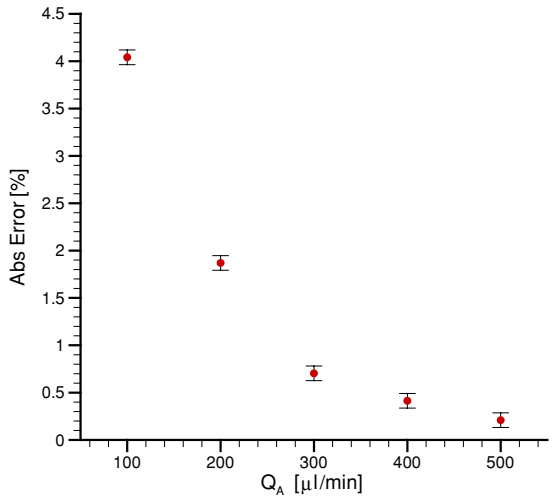


**Figure 7.** Verification of interface tracking sensor reading against the standard syringe pump. The flow Reynolds number of pressure-driven flow varied from 0.7716 to 3.858.

from the microfluidic sensor are very close to the input values of the syringe pump. It is interesting to note that the error in experimental results approaches 1% at higher flow rates, but the difference between $Q_S$ and $Q_A$ remains almost identical at all flow rates. This could be attributed to the bias error or initial offset of the syringe pump. Also at low flow rates, the syringe pump readings are more unreliable due to the intermittent driving mechanism of the gear pump. Another source of error could be the evaporation of the working fluid, although we placed oil on the free surface of exit reservoir. The absolute error in the flow rate measurement is estimated to be within 3.8 $\mu$l min$^{-1}$, which is very small compared to experimental results presented in figure 7.

## 5. Summary and conclusions

A conductivity-based interface tracking method is presented for measuring the marching flow velocity of a liquid–gas boundary as the microchannel is filled with liquid. A microchannel network is formed on PDMS using soft lithography, while all electrodes are deposited on a glass substrate. This on-chip interface tracking sensor is capable of measuring an ultra low flow velocity developed during electroosmotic and mixed electroosmotic-pressure-driven flows. The accuracy of the conductivity-based interface tracking method is verified with that of optical methods.

In this study, induced pressure head from a planar electrokinetic micropump is used to drive/fill liquid in hybrid microfluidic channels. Electrokinetic-induced pressures are generated at different electric field strengths. For a particular microfluidic channel and electrolyte condition, the electroosmotically induced pressure increases with the electric field. The velocity of the liquid–gas interface decreases as the liquid travels along the unwetted surface. Experiments show that the surface tension force was not big enough to fill the polymeric microchannel spontaneously, and it was easier to load the working fluid into thin microchannel using electroosmotic flows. The experimental flow velocity obtained from this sensor is also compared with that of a one-dimensional flow model. Here it is assumed that at any particular time the flow velocity remains constant in the entire wetted region. The one-dimensional flow model can predict the marching velocity within the experimental error bars, especially at low electric field.

## Acknowledgments

This investigation was supported in part by the Washington Technology Center, Seattle, WA, and in part by the National Science Foundation under Grant No. CTS0300802. The technical support provided by Robert Lenz and John Yates is greatly appreciated.

## References

[1] Xia Y and Whitesides G M 1998 Soft lithography *Annu. Rev. Mater. Sci.* **28** 153–84
[2] Culbertson C T, Ramsey R S and Ramsey J M 2000 Electroosmotically induced hydraulic pumping on microchips: differential ion transport *Anal. Chem.* **72** 2285–91
[3] Ericsson D and Li D 2004 Integrated microfluidic devices *Anal. Chim. Acta* **507** 11–26
[4] Rossier J, Reymond F and Michel P E 2002 Polymer microfluidic chips for electrochemical and biochemical analyses *Electrophoresis* **23** 858–68
[5] Wu S, Lin Q, Yuen Y and Tai Y C 2001 MEMS flow sensors for nano-fluidic applications *Sensors Actuators* A **89** 152–8
[6] Norlin P, Ohman O, Ekstrom B and Forssen L 1998 A chemical micro analysis system for the measurement of pressure, flow rate, temperature, conductivity, UV-absorption and fluorescence *Sensors Actuators* B **49** 34–9
[7] Bedo G, Fannasch H and Muller R 2000 A silicon flow sensor for gases and liquids using AC measurements *Sensors Actuators* A **85** 124–32
[8] Park H, Pak J J, Young-Son S, Lim G and Song I 2003 Fabrication of a micro channel integrated with inner sensors and the analysis of its laminar flow characteristics *Sensors Actuators* A **103** 317–29
[9] Baar J J V, Wiegerink R J, Lammerink T S J, Krijnen G J M and Elwenspoek 2001 Micromachined structures for the thermal measurements of fluid and flow parameters *J. Micromech. Microeng.* **11** 311–8
[10] Okulan N, Henderson H T and Ahn C H 2000 A pulsed mode micromachined flow sensor with temperature drift compensation *IEEE Trans. Electron Devices* **47** 340–8
[11] Ferreira H A, Grahan D L, Parracho P, Soares V and Freitas P P 2004 Flow velocity measurement in microchannels using magnetroresistive chips *IEEE Trans. Magn.* **40** 2652–4
[12] Sobolev V D, Churaev N V, Velarde M G and Zorin Z M 2000 Surface tension and dynamic contact angle of water in thin quartz capillaries *J. Colloid Interface Sci.* **222** 51–4
[13] Jones T B 2002 On the relationship of dielectrophoresis and electrowetting *Langmuir* **18** 4437–43
[14] Kang K H, Kang I S and Lee C M 2003 Wetting tension due to Coulombic interaction in charge-related wetting phenomena *Langmuir* **19** 5407–12
[15] Yang L J, Yao T and Tai Y 2004 The marching velocity of the capillary meniscus in a microchannel *J. Micromech. Microeng.* **14** 220–5
[16] Tas N R, Haneveld J, Jansen H V, Elwenspoek M and van den Berg A 2004 Capillary filling speed of water in nanochannels *Appl. Phys. Lett.* **85** 3274–6
[17] Kawaji M and Chung P M-Y 2004 Adiabatic gas–liquid flow in microchannels *Microscale Thermophys. Eng.* **8** 239–57

[18] Li H Y, Tseng F G and Pan C 2004 Bubble dynamics in microchannels: Part II. Two parallel microchannels *Int. J. Heat Mass Transfer* **47** 5591–601
[19] Clements M R 2003 Microfluidic handling on a thermally responsive surface *MS Thesis* (Seattle, WA: University of Washington)
[20] Hetsroni G, Klein D, Mosyak A, Segal Z and Pogrebnyak E 2004 Convective boiling in parallel microchannels *Microscale Thermophys. Eng.* **8** 403–21
[21] Srivastava N, Davenport R D and Burns M A 2005 Nanoliter viscometer for analyzing blood plasma and other liquid samples *Anal. Chem.* **77** 383–92
[22] Probstein R F 1994 *Physiochemical Hydrodynamics: An Introduction* 2nd edn (New York: Wiley)
[23] Dutta P, Warburton T C and Beskok A 2002 Numerical simulation of mixed electroosmotic/pressure driven flows *Numer. Heat Transfer* A **41** 131–48
[24] Kovacs G T A 1998 *Micromachined Transducers Source Book* (New York: WCB/McGraw-Hill)
[25] Becker H and Locascio L E 2002 Polymer microfluidic devices *Talanta* **56** 267–87
[26] Duffy D C, McDonald J C, Schueller J A and Whitesides G M 1998 Rapid prototyping of microfluidic systems in poly(dimethylsiloxane) *Anal. Chem.* **70** 4974–84
[27] Unger M A, Chou H P, Thorsen T, Scherer A and Quake S R 2000 Monolithic microfabricated valves and pumps by multilayer soft lithography *Science* **288** 113–6
[28] Gillmor S D, Thiel A J, Strother T C, Smith L M and Lagally M G 2000 Hydrophilic/hydrophobic patterned surfaces as templates for DNA arrays *Langmuir* **16** 7223
[29] Coleman H W and Steele W G 1998 *Experimentation and Uncertainty Analysis for Engineers* 2nd edn (New York: Wiley Interscience)
[30] Kline S J and McClintock F A 1953 Describing uncertainties in single sample experiments *Mech. Eng.* **75** 3–8
[31] Dutta P and Beskok A 2001 Analytical solution of combined electroosmotic/pressure driven flows in two-dimensional straight channels: finite Debye layer effects *Anal. Chem.* **73** 1979–86
[32] Santiago J G 2001 Electroosmotic flows in microchannels with finite inertial and pressure forces *Anal. Chem.* **73** 2353–65
[33] Horiuchi K and Dutta P 2005 Flow diagnosis in a trapezoidal microchannel *Proc. JSME Conf. on Fluid Mechanics* Paper No. AM05-07-002
[34] Xuan X, Xu B, Sinton D and Li D 2004 Electroosmotic flow with Joule heating effects *Lab Chip* **4** 230–6